journal

J. Am. Ceram. Soc., 78 [3] 513–20 (1995)

Cyclic Fatigue in Ceramics: A Balance between Crack Shielding Accumulation and Degradation

David S. Jacobs* and I-W. Chen*

Department of Materials Science and Engineering, University of Michigan, Ann Arbor, Michigan 48109-2136

Cyclic fatigue growth rates in *R*-curve ceramics have been observed to depend very strongly on the maximum applied stress intensity, K_{max}, and only weakly on the stress intensity range, ΔK. This behavior is rationalized through measurement of crack wake shielding characteristics as a function of these fatigue parameters in a gas-pressure-sintered silicon nitride. In particular, evidence for a mechanical equilibrium between shielding accumulation by crack growth and shielding degradation by frictional wear of sliding interfaces is found for steady-state cyclic fatigue. This equilibrium gives rise to a rate law for cyclic fatigue. The data suggest that the accumulation process is the origin of the strong K_{max} dependence, and that the degradation process is the origin of the weak ΔK dependence. These features are shown to be related to the "cyclic" *R*-curve and to the cyclic crack opening displacement, respectively.

I. Introduction

STABLE crack growth under cyclic loading has been observed in many ceramics which exhibit rising toughness (*R*-curve) behavior. Crack growth rates in these materials are seen to depend strongly on the maximum applied stress intensity, K_{max}, and rather weakly on the stress intensity range, ΔK. Specifically, Liu and Chen[1] have found that a modified Paris Law of the form

$$da/dt = A(K_{max})^n (\Delta K)^m \quad (1)$$

best describes fatigue data for Y-TZP, with $n = 19$ and $m = 2$. A similar strong K_{max} and weak ΔK dependence was found by Dauskardt *et al.*[2,3] for an Al_2O_3/SiC_w composite. This behavior contrasts with that of metals and polymers, for which crack growth is governed mainly by ΔK.[4] One would expect that the different behavior of brittle and ductile materials in fatigue is related to the micromechanics of crack growth.

Under monotonically increasing loads, stable crack growth in ceramics is associated with mechanisms which shield the crack tip from the applied load. Frictional pullout of grains or secondary phases in the crack wake has been identified as a dominant shielding mechanism at low temperatures for nontransformable ceramics.[5–14] The *R*-curve results from the accumulation of shielding as the crack grows and the wake zone increases in size. Furthermore, the interfacial frictional force, τ, has been identified as the key parameter governing the shielding capacity of the crack wake zone.[7,11–13,15] This τ can arise from such sources as thermal expansion anisotropy,[7,11–13,15,16] surface roughness,[16–18,19] or geometric interlocking.[7,11,20]

Compelling evidence indicates that degradation of crack shielding, or τ, occurs during cyclic loading of these materials. A decrease in τ during cyclic fatigue was inferred by Lathabai *et al.*[21] from *in situ* observations of wear debris at frictional interfaces in monolithic Al_2O_3. Evidence confirming this has been reported in cyclic fatigue tests of glass ceramic/SiC fiber composites.[22,23] In addition, a decrease in τ due to reverse or fatigue loading has been well documented through fiber push-down and pushthrough tests in ceramic matrix composites.[17,19,24] Furthermore, Hu and Mai[25] have measured an increase in specimen compliance during cyclic loading of Al_2O_3, which they attributed to shielding degradation due to interfacial sliding.

As yet, however, the link between shielding degradation and fatigue kinetics has not been established. Moreover, the separate ΔK and K_{max} dependencies in Eq. (1) suggest that multiple mechanisms are active in cyclic fatigue. One possibility is that static fatigue, an environmentally activated process sensitive to K_{max}, operates along with shielding degradation. However, this is not consistent with reports that cyclic fatigue can occur even in the absence of measurable static fatigue.[26,27] In addition, the K_{max} sensitivity of static fatigue is usually much higher than that seen in cyclic fatigue,[27] and it would be expected to be higher still if concurrent shielding degradation were occurring. Finally, if mechanisms such as these were acting in series or in parallel, a transition between ΔK control and K_{max} control would result, not a multiplicative law such as Eq. (1). So, although environmental interactions have been shown to affect cyclic fatigue,[26–28] this mechanism appears incapable of explaining the observed kinetics.

An alternative explanation has been suggested by Hu and Mai,[25] who postulate that crack growth in cyclic fatigue maintains a mechanical equilibrium between the degradation in shielding due to cyclic damage in the wake zone and the addition of shielding at the growing crack tip. In this paper, we more fully develop the idea of such a mechanical equilibrium and explore its implications for cyclic fatigue in ceramics. Experimental evidence consistent with this concept is sought, using a high-toughness silicon nitride. Values are obtained for shielding accumulation and degradation rates in this material, and the data suggest unique K_{max} and ΔK dependencies for these processes. When taken together, these dependencies can account for the characteristic fatigue equation given by Eq. (1).

II. Theoretical Development

We assume here that fatigue crack growth is a continuous process which, under steady-state conditions, proceeds with a constant shielding stress intensity, K_{sh}, for a given applied K_{max} and *R*-ratio (K_{min}/K_{max}). We also assume that the crack will propagate only when the stress intensity at the crack tip exceeds the intrinsic toughness, K_0, of the material. In this case, the applied K needed to cause propagation, K_{appl}, must be

$$K_{appl} = K_0 + K_{sh} \quad (2)$$

Under monotonic loading, K_{sh} normally increases during crack growth if the shielding zone is not fully evolved, as evidenced by the *R*-curve. Under cyclic loading, we assume that K_{sh} may increase or decrease, but that a steady-state K_{sh} may be reached so that the crack grows at a constant velocity under conditions of constant (K_{max}, K_{min}). This is possible if, at steady state, there is a cyclic-loading-induced degradation of K_{sh} that balances the accumulation of K_{sh} due to crack growth.

R. Raj—contributing editor

Manuscript No. 193735. Received March 17, 1994; approved September 6, 1994.
Supported by the U.S. Air Force Office for Scientific Research under Grant No. AFOSR-91-0094.
*Member, American Ceramic Society.

To physically model this process, we consider that an increase in K_{sh} is accomplished by propagating the crack an increment, da, while a decrease in K_{sh} is obtained by allowing the grains in the shielding zone to undergo frictional sliding over a period of time, dt. At equilibrium, these accumulation and degradation processes balance so that the net change in shielding, dK_{sh}, is zero, and this can be written as

$$dK_{sh} = \frac{\partial K_{sh}}{\partial a} da + \frac{\partial K_{sh}}{\partial t} dt = 0 \quad (3)$$

By rearranging, we obtain

$$\frac{da}{dt} = \left(\frac{-\partial K_{sh}}{\partial t}\right)\left(\frac{\partial K_{sh}}{\partial a}\right)^{-1} \quad (4)$$

Thus, under steady-state conditions, *this equilibrium naturally leads to a cyclic fatigue rate law.*

In Eqs. (3) and (4), $\partial K_{sh}/\partial a$ and $\partial K_{sh}/\partial t$ are the shielding accumulation and degradation rates, respectively. If these terms can be shown to have unique dependencies on K_{max} and ΔK, then Eq. (4) becomes equivalent to Eq. (1) in form. If these K_{max} and ΔK dependencies are also found to be equivalent to those for da/dt, then we have strong evidence that the competition between shielding accumulation and degradation is the primary mechanism for cyclic fatigue in our materials.

In this study, we have independently measured da/dt, $\partial K_{sh}/\partial a$, and $\partial K_{sh}/\partial t$ and their dependencies on K_{max} and ΔK for an *in situ* toughened Si_3N_4. The data validate Eq. (4) and the postulated mechanism for steady-state cyclic fatigue. The strong K_{max} dependence of da/dt is found to arise from $\partial K_{sh}/\partial a$ and can be linked to R-curve behavior, while the weak ΔK dependence arises from $\partial K_{sh}/\partial t$ and is associated with the frictional wear of sliding interfaces.

III. Experimental Procedures

(1) Materials

Standard compact tension (CT) specimens (W = 25 mm, B = 3.50 mm) were fabricated from a gas-pressure-sintered β-silicon nitride. The starting powder contained 10 wt% (Y_2O_3 + Al_2O_3) as sintering aids. The material was sintered at 1900°C for 5 h in N_2 at 10 atm pressure. The resulting microstructure contains randomly oriented, elongated β-Si_3N_4 grains embedded in an intergranular glass phase. Grain lengths range from 1.5 to 40 μm and widths from 0.5 to 4 μm. Several important material properties are E = 300 GPa, H = 14 GPa, and $K_{IC} \approx$ 7.5 MPa·m$^{1/2}$ (estimated plateau of R-curve).

(2) Crack Length Measurement

Crack lengths were monitored *in situ* during testing using a dc electric potential (DCEP) technique. A thin Ti film (≈0.1 μm) was evaporated onto one face of the CT specimen, and a digital multimeter was used to monitor the film resistance and relay these data to the controlling computer. The absolute crack lengths on the front and back faces were measured before and after each test, using a micrometer stage and an optical microscope. The average of these was used as the "true" crack length, with an uncertainty of about ±5 μm. However, much smaller *increments* in crack growth could be resolved using the DCEP technique. Calibrations of the Ti film showed that for every 10 μm of crack growth, the film resistance increased by about 1 Ω. Since the resistance was known to a resolution of 0.01 Ω, crack increments on the order of 0.1 μm can theoretically be resolved by our system. In practice, some uncertainty in the DCEP measurement is introduced, due to the meandering nature of the crack and the possibility of incomplete separation of crack faces in the wake zone. We therefore limit our resolution for Δa to 0.5 μm.

(3) Cyclic Fatigue/R-Curve Tests

Prior to testing, all specimens were precracked to yield long cracks (a > 6 mm). All testing generally utilized a two-step process. First, the crack was allowed to reach a steady-state growth rate under a given set of cyclic fatigue parameters (i.e., K_{max}, R-ratio, and frequency; see below). Steady state was generally obtained within 150 to 200 μm of crack extension. In the second step, the initial portion of the R-curve was measured under a monotonically increasing load to characterize either $\partial K_{sh}/\partial a$ or $\partial K_{sh}/\partial t$. This two-step process was then repeated for a different set of cyclic fatigue conditions. Cyclic fatigue was performed under load control using a closed-loop servohydraulic test system (MTS). Monotonic loading was performed under strain control, utilizing an axial extensometer attached to the crack mouth.

Three types of tests, shown schematically in Fig. 1, were performed to probe the characteristics of fatigue kinetics (i.e., da/dt) and shielding accumulation and degradation.

(A) K_{max} Dependencies of da/dt and $\partial K_{sh}/\partial a$: The crack was first propagated in cyclic fatigue at a constant K_{max} in the range of 5.50 to 6.52 MPa·m$^{1/2}$, with the R-ratio and frequency set at R = 0.1 and f = 4 Hz. After measuring the R-curve under monotonic loading to determine $\partial K_{sh}/\partial a$, a different K_{max} was chosen, and the test was repeated using the same R-ratio and frequency. In this way, the K_{max} dependencies of da/dt and $\partial K_{sh}/\partial a$ could ultimately be determined.

(B) ΔK Dependencies of da/dt and $\partial K_{sh}/\partial a$: K_{max} was fixed at 6.25 MPa·m$^{1/2}$, and steady state was established under cyclic fatigue at 4 Hz for a constant R-ratio in the range $0.1 \leq R \leq 0.6$. The R-curve was measured after reaching steady state to determine $\partial K_{sh}/\partial a$, and then a different R-ratio was selected and the test sequence repeated. In this way, the ΔK dependencies of da/dt and $\partial K_{sh}/\partial a$ were obtained.

(C) K_{max} and ΔK Dependencies for $\partial K_{sh}/\partial t$: An R-curve test was first performed until a selected level of crack resistance ($K^* \approx$ 7.0 MPa·m$^{1/2}$) was developed. Next, the material was subjected to cyclic loading at 4 Hz for a selected number of cycles (generally between 1 000 and 50 000 cycles). Values of K_{max} and R-ratio were chosen such that *no crack growth would occur* during the cyclic fatigue test segment (K_{max} = 5.25 and 4.50 MPa·m$^{1/2}$ and $0.1 \leq R \leq 0.6$). This deactivates the accumulation process so the degradation process can be isolated and characterized. After cyclic fatigue, the R-curve was again measured, and the initial K at which crack growth was first observed, K_i, was identified. The net change in crack shielding, dK_{sh}, was then ($K^* - K_i$), which was divided by the time of

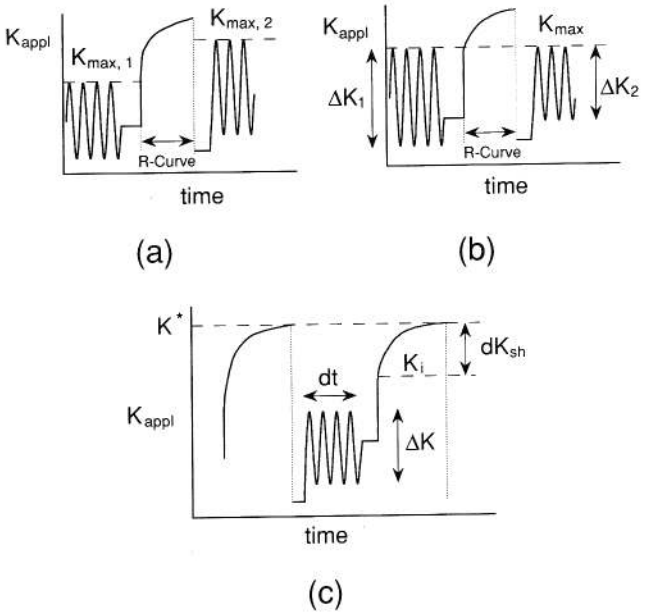

Fig. 1. Schematic of test procedures. (a) R-ratio fixed at R = 0.1, $5.55 \leq K_{max} \leq 6.52$; (b) K_{max} fixed at 6.25 MPa·m$^{1/2}$, $0.1 \leq R \leq 0.6$; (c) K_{max} fixed at 5.25 or 4.50 MPa·m$^{1/2}$, $0.1 \leq R \leq 0.6$ (no crack growth occurs during cyclic fatigue portion of this test). f = 4 Hz for all cyclic loading.

cyclic loading to give $\partial K_{sh}/\partial t$. By performing this test for different values of K_{max} and R, the dependencies of $\partial K_{sh}/\partial t$ on K_{max} and ΔK were obtained. Note that $\partial K_{sh}/\partial t$ is not obtained under steady-state conditions; however, this is not expected to alter the ΔK dependence significantly.

(4) Quantification of Shielding Accumulation Rates

To quantify shielding evolution, measured R-curves were fit by the equation

$$K_R = K_i (1 + \beta \Delta a)^p \quad (5)$$

Here K_R is the measured fracture resistance, K_i is the initial toughness at the onset of crack growth under monotonic loading, Δa is the crack growth increment, and β and p are constants. We note that the Taylor expansion of Eq. (5) yields

$$K_R = K_i + f(\Delta a) \quad (6)$$

where $f(\Delta a)$ describes the change in K_{sh} with Δa. In this sense, Eq. (5) is similar in physical meaning to Eq. (2). The initial slope of the R-curve, i.e., $\partial K_{sh}/\partial a$ is the first derivative of Eq. (5) at $\Delta a = 0$:

$$\frac{\partial K_{sh}}{\partial a} = \beta p K_i \quad (7)$$

This initial slope, found when the system is very slightly perturbed away from steady-state conditions, is the best available measurement for $\partial K_{sh}/\partial a$ during steady-state cyclic fatigue. Shielding degradation rates were also obtained from R-curve measurements, as described above.

IV. Results

(1) Crack Profile in Monotonic and Cyclic Loading

Figure 2 shows typical crack profiles for a long crack ($a >$ 8 mm) after loading (Fig. 2(a)) and after monotonic loading (Fig. 2(b)).The intergranular glass phase, which is yttrium-rich and thus appears brighter due to Z contrast, is also apparent. The regions shown in Figs. 2(a) and (b) are about 380 and 75 μm behind the crack tip, respectively, and were observed unloaded in the scanning electron microscope (SEM). A residual opening is observed in both micrographs, attesting to the load-bearing ability of the crack wake shielding zone. The region in Fig. 2(b) had been freshly produced during an R-curve test (Δa of this test was 180 μm) and had not experienced any cyclic loading.

The most significant feature distinguishing Figs. 2(a) and (b) is that wear debris is seen only at sliding interfaces in Fig. 2(a) (indicated by arrows). Fracture is seen to be mainly intergranular for both cyclic and monotonic loading, and sliding interfaces (i.e., grains undergoing frictional pullout) are apparent in both cases. Thus, the observed debris supports the belief that cyclic loading produces frictional wear at sliding grains and promotes shielding degradation.

(2) Steady-State Growing Rates in Cyclic Fatigue

(A) Establishing Steady State: The crack growth rate measured in cyclic fatigue (after prior monotonic loading to measure the R-curve) generally reached a steady-state value after a period of transient acceleration, as seen in Fig. 3. We interpret the transient region as an indication that K_{sh} decreases during cyclic loading relative to its value at the end of the R-curve test. Thus, as the crack grows under conditions of constant (K_{max}, K_{min}) in cyclic fatigue, a degradation of K_{sh} results in increasing growth rates. Furthermore, these data also suggest that shielding accumulation occurs during cyclic fatigue; otherwise the crack velocity would continue to increase at constant (K_{max}, K_{min}) until fast fracture occurs. Instead, a constant da/dt is obtained after about 200 μm of crack growth, and this is taken to be an indication that a mechanical equilibrium between shielding accumulation and degradation has been attained. The small oscillations around the steady-state growth rate seen in Fig. 3 may reflect an overshoot/undershoot process in which the surface crack alternately leads, then lags, the interior crack front. Further study is needed to confirm this.

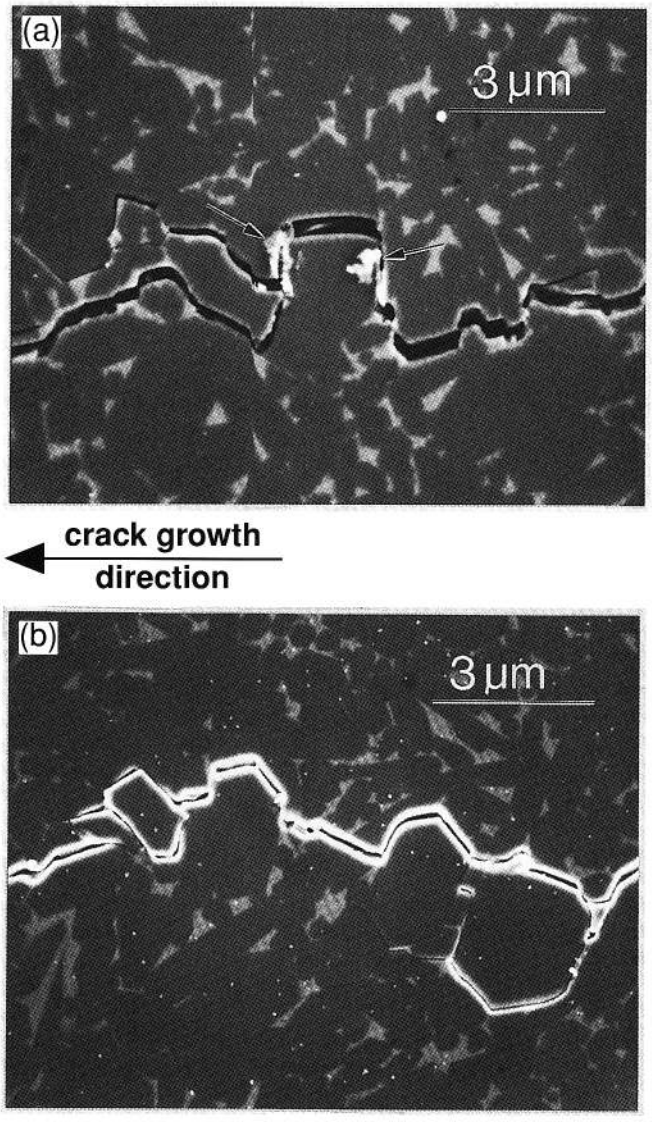

Fig. 2. Crack profile in Si_3N_4 after (a) cyclic fatigue; wear debris at the sliding interfaces is indicated by arrows, (b) propagation under monotonically increasing load.

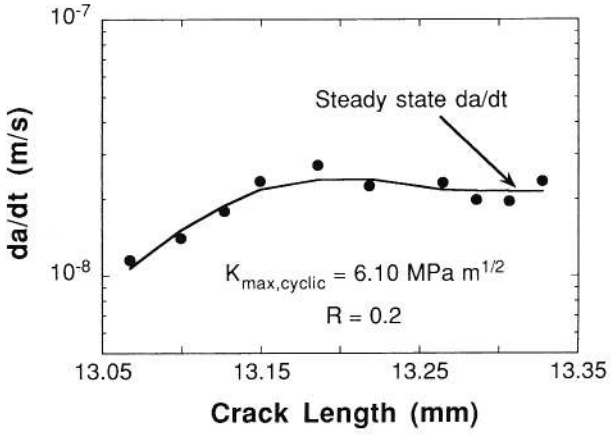

Fig. 3. Establishment of steady-state da/dt during cyclic fatigue at constant K_{max} and R-ratio. The crack had previously been propagated about 25 μm under monotonic loading to a peak K_R of 7.2 MPa·m$^{1/2}$.

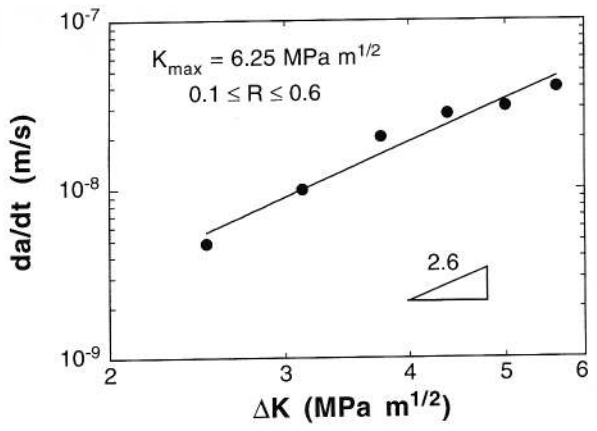

Fig. 4. ΔK dependence of steady-state cyclic fatigue growth rates.

(B) Dependence on ΔK: Figure 4 gives the dependence of steady-state da/dt on ΔK, from data obtained when tests were conducted at different R-ratios but at a fixed K_{max} (6.25 MPa·m$^{1/2}$; cf. Fig. 1(b)). The data are plotted on a log–log scale, and a power law exponent $m = 2.6 \pm 0.8$ is found from the curve fit. Our m value is consistent with other reports on silicon nitride[30,31] and other ceramics,[1,2,26] for which m is seen to be characteristically small, on the order of 2 to 3, over a wide range of K_{max}.

(C) Dependence on K_{max}: Figure 5 summarizes the steady-state growth rates measured under fixed R-ratio and frequency conditions (cf. Fig. 1(a)). These data are plotted against K_{max} on a log–log scale, and a power law curve fit yields an exponent of 21.6 ± 3.2. Referring to Eq. (1), and realizing that $\Delta K = (1 - R)K_{max}$, we see that

$$da/dt = A(1 - R)^m(K_{max})^{n+m} \tag{8}$$

and thus $n + m = 21.6$. Since $m = 2.6$ from above, we see that $n = 19 \pm 3.2$ in Eq. (1). This strong K_{max} dependence of da/dt is consistent with other reports on cyclic fatigue in silicon nitride[30,31] and in other ceramics.[1,2,26]

(3) Shielding Accumulation from R-Curve Measurements

Figure 6 shows examples of the initial R-curves obtained by monotonic loading after establishing steady-state shielding in cyclic fatigue. The position and shape of the R-curve is clearly influenced by the cyclic fatigue portion of the test. The first increment of crack growth is seen at $K_R = K_{max}$ used in the preceding cyclic loading, within experimental error. In addition, the initial slope of the R-curve, $\partial K_{sh}/\partial a$, is seen to decrease as the cyclic K_{max} was increased.

On the other hand, changing the R-ratio from 0.1 to 0.6 at $K_{max} = 6.25$ MPa·m$^{1/2}$ does not significantly affect $\partial K_{sh}/\partial a$. As seen in Fig. 7, the K_i and the *initial* slope for different R-ratios are relatively consistent. There appears to be a tendency for the curves to rise more strongly at higher R, suggesting that the details of crack wake shielding are not fully independent of ΔK. However, since no systematic dependence is apparent for K_i or $\partial K_{sh}/\partial a$, we conclude that, to a first approximation, shielding accumulation at $\Delta a = 0$ depends mainly on K_{max} and not on ΔK.

By fitting the R-curves to Eq. (5) and evaluating the initial slopes at $K_R = K_{max}$ (i.e., $\Delta a = 0$), we obtain $\partial K_{sh}/\partial a$ (the curve fits are shown by solid lines in Fig. 6). These $\partial K_{sh}/\partial a$ are plotted in Fig. 8 against K_{max}. A power law curve fit yields an exponent of $n = 18 \pm 6.5$ showing that shielding accumulation is a strong function of K_{max}. This K_{max} dependence is consistent with the value of n reported above for da/dt, suggesting that the strong K_{max} dependence of cyclic fatigue originates from the shielding accumulation process.

To be convincing that our R-curves and measured $\partial K_{sh}/\partial a$ values are reasonable for ceramic materials, a comprehensive review of R-curve data for a variety of materials is given in Table I. At large values of Δa, the slope of our R-curves certainly appears typical (our R-curves were extrapolated to $\Delta a = 500$ μm for this comparison). At smaller values of Δa, the very steep rise seen at the beginning of our R-curves has also been reported for indentation–strength tests on Si_3N_4[32] and Al_2O_3,[33,34] and in theoretical predictions and notched beam tests for ZrO_2.[35] Other tests utilizing CT or similar geometries do not report such high slopes.[7,8,10,14,26,36] However, these tests generally used crack measurement techniques with insufficient resolution to collect data at very small Δa. (The *in situ* SEM studies of crack growth have no such limitation; however, these studies[7,8] did not report data at very small Δa, and in Ref. 8 the R-curve is calculated rather than directly measured from Δa-load data. Thus, even the SEM studies do not provide conclusive data for the initial portion of the R-curve.)

We have further confirmed the steep initial slope in our data by careful optical measurements done *in situ* using a high-power microscope/video recording system (≈1000X magnification). These measurements show that, after cyclic fatigue at $K_{max} = 6.25$ MPa·m$^{1/2}$, the initial $\partial K_{sh}/\partial a$ of the R-curve is at least 1.8×10^5 MPa·m$^{-1/2}$. Thus, it appears that the very steep initial slope of our R-curves is a real phenomenon in ceramics.

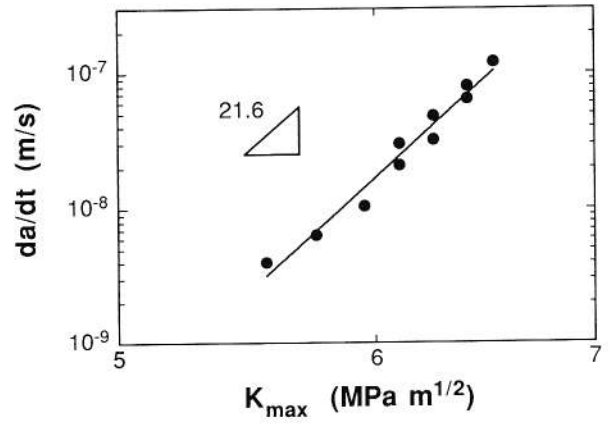

Fig. 5. Steady-state cyclic fatigue growth rates observed at various K_{max} ($R = 0.1$).

(4) Shielding Degradation

Evidence for shielding degradation during cyclic fatigue has already been presented in Fig. 3 by the transient acceleration in crack growth rates during cyclic loading. More directly, shielding degradation rates, $\partial K_{sh}/\partial t$, were measured as described in Section III(3), above. These results are plotted in Fig. 9 as a function of ΔK. Note that these data were obtained for two values of K_{max}, and that no effect of K_{max} is apparent in Fig. 9.

The power law exponent from Fig. 9 giving the dependence of $\partial K_{sh}/\partial t$ on ΔK is $m = 2.9 \pm 0.7$. According to Eq. (4), this dependence can account for the observed ΔK dependence of da/dt (Section IV(2)(B), indicating that the weak ΔK dependence of cyclic fatigue originates from the shielding degradation process.

(5) Confirmation of Fatigue Mechanism

Using the *independently* measured values for $\partial K_{sh}/\partial a$ and $\partial K_{sh}/\partial t$ in Figs. 8 and 9, we have calculated da/dt using Eq. (4) for various K_{max} at $R = 0.1$ (thus both K_{max} and ΔK are varied). A comparison with the measured steady-state growth rates is shown in Fig.10. The computed values are generally within one order of magnitude of the experimentally observed da/dt. This is very reasonable, given the fact that the values for $\partial K_{sh}/\partial t$ used in the calculations were measured for a freshly generated rather than a steady-state cyclic shielding zone. Thus the calculated

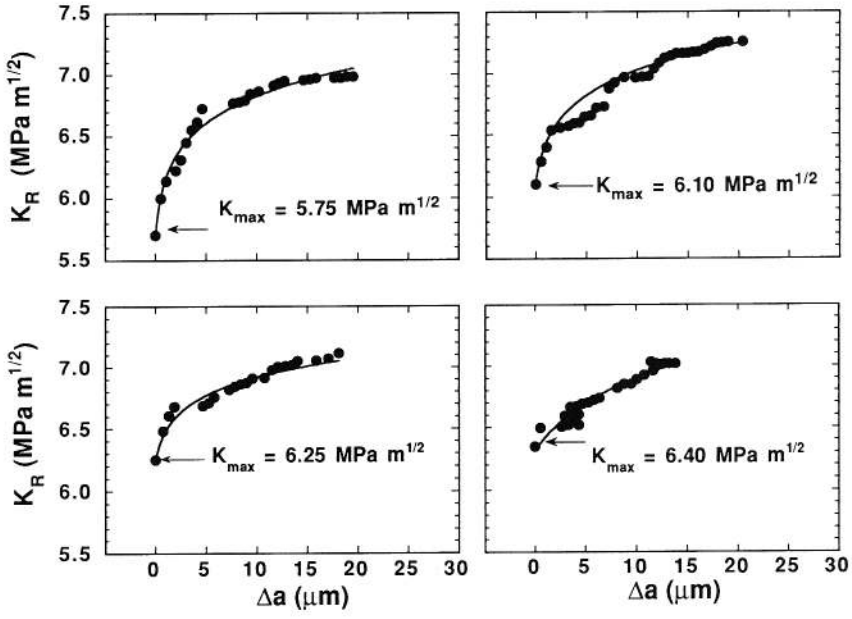

Fig. 6. Effect of K_{max} during cyclic fatigue (at $R = 0.1$) on the initial R-curve. Solid lines show curve fit to Eq. (5).

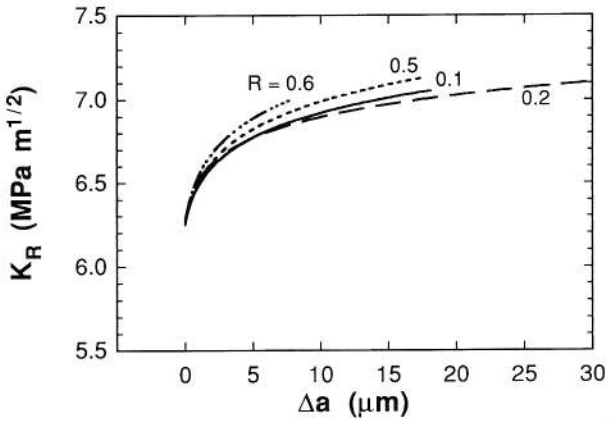

Fig. 7. Comparison of initial R-curves at $K_{max} = 6.25$ MPa·m$^{1/2}$ and various R-ratios.

Table I. Typical Values of $\partial K_R/\partial a$ from R-Curve Measurements

Material	Initial $\partial K_R/\partial a$	$\partial K_R/\partial a$ at 500 μm (MPa·m$^{1/2}$)	Ref.
Si_3N_4	8×10^4 to 2×10^6	3.5×10^3	This paper
	8×10^3	5.2×10^3	36
	9×10^4	2.6×10^3	32†
	3.4×10^3	2.3×10^3	10
	1×10^3	1×10^3	39
ZrO_2	1×10^4	2.8×10^3	26‡
	1.7×10^6 to 9×10^4	0 to 2.8×10^3	35
Al_2O_3	1×10^5 to 8×10^5	0 to 320	33
	1×10^3	1×10^3	7
	2×10^3	1×10^3	8
	1.3×10^6	3702×10^3	34
	2×10^3		37
SiC_w/Al_2O_3	2.5×10^4	1.5×10^3	38
	5×10^3	4×10^3	29

†Interpreted data differently from original authors. ‡Mid-toughness ZrO_2.

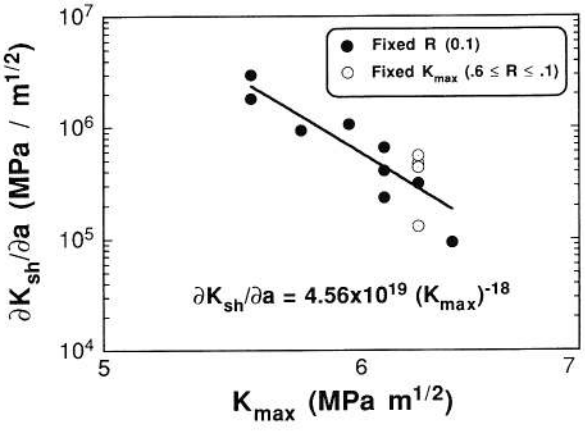

Fig. 8. Dependence of $\partial K_{sh}/\partial a$ (initial slope of the R-curve) on the prior K_{max} used to reach steady state during cyclic fatigue.

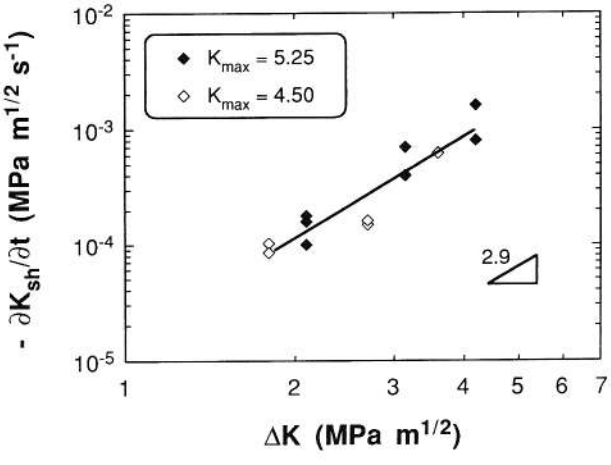

Fig. 9. Measured dependence of $\partial K_{sh}/\partial t$ on ΔK.

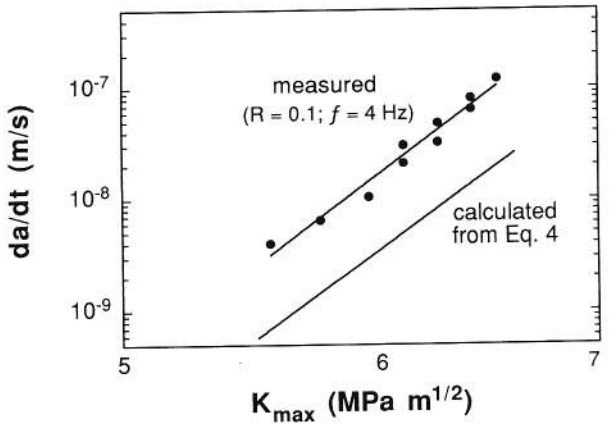

Fig. 10. Comparison of measured da/dt values with those calculated from Eq. (4) using independently measured values for $\partial K_{sh}/\partial a$ and $\partial K_{sh}/\partial t$.

da/dt would be expected to differ somewhat from the steady-state data. Furthermore, the slopes of the measured and calculated curves are nearly identical, as one would expect. Thus, these data appear to be self-consistent within the accuracy of fatigue crack growth measurements, and the fatigue mechanism represented by Eq. (4) appears to be very credible.

V. Discussion

The rate law expresed in Eq. (4), from consideration that $dK_{sh} = 0$ at steady state, represents a decoupling of K_{max} and ΔK dependent processes that is equivalent to the empirical rate law in Eq. (1). From our results, this is seen in three ways. First, the shielding accumulation process, $\partial K_{sh}/\partial a$, is a strong, decreasing function of K_{max} and is primarily responsible for the strong K_{max} dependence of da/dt. Second, the shielding degradation process, $\partial K_{sh}/\partial t$, is a weak, increasing function of ΔK and is primarily responsible for the weak ΔK dependence of da/dt. Third, the power law exponents found for these two processes combine to yield the proper relationship for da/dt, within experimental error. Table II summarizes the n and m values measured independently for fatigue kinetics and for crack shielding, along with the 95% confidence interval for each. The conceptually appealing decoupling between K_{max} and ΔK dependent processes suggested by the above considerations is further rationalized below.

(1) Accumulation of Shielding

If the "state" of shielding during cyclic fatigue is related to the R-curve, then the inverse dependence of the shielding accumulation process, $\partial K_{sh}/\partial a$, on K_{max} is not surprising. A typical R-curve in ceramics has a concave downward curvature and reaches a plateau, K_∞, after a sufficiently large amount of crack growth. We recall from Section IV(3) that, after reaching steady state in cyclic fatigue at constant K_{max}, the first crack growth in subsequent monotonic loading occurred near this K_{max}. We can therefore assume that, for our experiments, K_{max} corresponds to a point on the R-curve, K_R. Thus, if the applied K_{max} during cyclic fatigue is near K_0, then $\partial K_{sh}/\partial a$ should follow the steeply rising portion of the R-curve, whereas if the applied K_{max} is near K_∞, then $\partial K_{sh}/\partial a$ should follow the plateau region.

Indeed, one can mathematically derive a "cyclic" R-curve resembling the experimental curves from the power law fit to the data in Fig. 8. We can write

$$\frac{\partial K_{sh}}{\partial a} = \frac{dK_R}{d(\Delta a)} = A(K_R)^{-n} \tag{9}$$

and by integrating find that

$$K_R = [K_0^{(n+1)} + (n+1)A\,\Delta a]^{1/(n+1)} \tag{10}$$

The above expression gives the R-curve a concave downward shape for $n \geq 1$ and is the same form as Eq. (5) if we factor the K_0 term out of the brackets. We can then calculate the "cyclic" R-curve using $n = 18$ and $A = 4.56 \times 10^{13}$ (from the curve fit in Fig. 8, with units adjusted to micrometers), and $K_0 = 4.0$ MPa·m$^{1/2}$ (from K_{IC} measurements of low-toughness Si_3N_4, which has mainly equiaxed rather than elongated grains[39, 40]). Note that this "cyclic" R-curve is actually the locus of the initial $\partial K_{sh}/\partial a$ values found from the R-curves obtained after establishing steady-state cyclic fatigue. In this context, it is analogous to the "cyclic" stress–strain curve (as opposed to the monotonic stress–strain curve) in the fatigue literature.[41]

In Fig. 11 we plot the calculated "cyclic" R-curve along with two monotonic curves measured after cyclic fatigue at $R = 0.1$ (nearly all the R-curves measured in this study fall in the band between these two curves). The two monotonic curves have been shifted along the Δa axis so their origins, i.e., their K_i, lie on the "cyclic" R-curve. We see that initially the agreement between these R-curves is good, but that the "cyclic" R-curve deviates from the monotonic R-curves as Δa increases. Note that cyclic fatigue tests could not be performed above $K_{max} \approx$ 6.6 MPa·m$^{1/2}$ (because specimen failure would occur), so above this point, the "cyclic" R-curve is an extrapolation of the actual data. In addition, it is seen that after fatigue at lower K_{max}, the monotonic R-curve diverges earlier from the "cyclic" R-curve.

The reason for the discrepancies between the "cyclic" and monotonic R-curves is not readily apparent. One may speculate that the physical reason arises from load history effects. If the wake zone is previously degraded, as it is after cyclic fatigue, then adding new bridges at the crack tip may have a more pronounced contribution to K_{sh} than would be seen in an undegraded wake zone having the same initial K_{sh}. Since the "cyclic" R-curve represents the response of adding bridges to a degraded shielding zone at various K_{max}, it would be expected to deviate from the monotonic curves, which are dominated by an undegraded shielding zone, especially as Δa increases. Different traction distributions in the wake zone after fatigue at high and at low K_{max} are also expected, since in the latter case da/dt is

Table II. Summary of K_{max} and ΔK Dependencies†

Measurements of fatigue kinetics		Measurements of shielding	
n (da/dt vs K_{max})	m (da/dt vs ΔK)	n ($\partial K_{sh}/\partial a$ vs K_{max})	m ($\partial K_{sh}/\partial t$ vs ΔK)
19 ± 3.2	2.6 ± 0.8	18 ± 6.5	2.9 ± 0.7

†Including 95% confidence intervals.

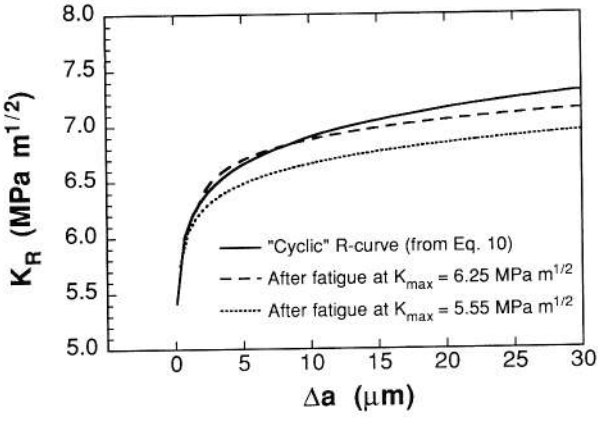

Fig. 11. Comparison of monotonic R-curves with the "cyclic" R-curve calculated from Eq. (10) using the parameters found in Fig. 8.

small and sliding grains spend more time in the wake zone. This may help explain the differences seen between the two monotonic curves in Fig. 11 as well. The numerical or analytical treatment needed to resolve these issues is beyond the scope of this paper.

(2) Degradation of Shielding from Frictional Sliding

In this section we will argue that, theoretically, a weak ΔK dependence for $\partial K_{sh}/\partial t$ (and thus for da/dt) is reasonable. For a frictional pullout mechanism, the shielding energy, ΔG, is given by[40]

$$\Delta G = V_f \tau \left(\frac{L^2}{R}\right) \tag{11}$$

Here τ is the shear stress at the interface, L is the sliding length, R is the radius of the grain undergoing pullout, and V_f is the volume fraction of grains participating in shielding. The shielding stress intensity factor, K_{sh}, in plane strain is thus[40]

$$K_{sh} = \sqrt{E'(G_0 + \Delta G)} - \sqrt{E' G_0} \tag{12}$$

where E' is Young's modulus in plane strain and G_0 is the energy release rate for a crack with no shielding (corresponding to the base toughness of the material, K_0) and is a constant. The variable of interest in the ΔG term is τ (the other parameters are assumed to be fixed by the microstructure in this analysis). This τ has been found to decrease in value with reverse or multiple loadings.[17,19,22–24] Therefore, we can relate the shielding degradation process to degradation of τ through the expression

$$\frac{\partial K_{sh}}{\partial t} = \frac{\partial K_{sh}}{\partial \tau}\frac{\partial \tau}{\partial u}\frac{du}{dt}$$

$$= \frac{\partial K_{sh}}{\partial \tau}\frac{\partial \tau}{\partial u}(f)(\Delta u) \tag{13}$$

Here, Δu represents the amplitude of sliding distance, or crack opening displacement, experienced in the shielding zone during cyclic loading, and f is the cyclic frequency.

Inspection of Eq. (13) reveals that the ΔK dependence of $\partial K_{sh}/\partial t$ arises from the Δu term. The first term, $\partial K_{sh}/\partial \tau$, can be found from Eqs. (11) and (12) and depends only on G_0 and τ; the second term, $\partial \tau/\partial u$, can be approximated by

$$\frac{\partial \tau}{\partial u} = -k'\tau \tag{14}$$

where k' is a constant related to the wear coefficient, Young's modulus, and the radius of a grain (see Appendix); and the third term, f, is a constant. Therefore, the only term with a ΔK dependence is Δu.

We do not attempt an exact solution for Δu here. However, several relationships exist in the literature suggesting that a weak dependence of Δu on ΔK is expected. For instance, in a material with no wake shielding, Δu at any point along the crack profile varies proportionally with the applied ΔK according to the Irwin relation.[8] For the case of a single bridging fiber,[15,24,42] Δu has been shown to be proportional to ΔK.[2] Shielding by frictional pullout is expected to be an intermediate case, since the traction acting to close the crack varies between that of an elastic bridge (when $u = u_{min}$) and zero (when the grain is pulled completely out of its socket at $u = u_{critical}$). However, for long cracks there are many grains undergoing pullout in the crack wake, and this introduces a set of complex interactions that could also affect the ΔK dependence of Δu. A more explicit understanding of frictional pullout for a realistic wake zone undergoing reverse loading, and of other effects such as changes in sliding geometry and crack closure with progressive wear, is needed to fully understand the ΔK dependence described by the data. Nevertheless, a weak ΔK dependence for shielding degradation by a frictional pullout mechanism is generally expected, based on the above considerations.

(3) Final Comments

The mechanical equilibrium process represented by Eq. (3) is believed to be a fundamental feature of cyclic fatigue in both monolithic and reinforced ceramic materials which possess wake shielding and rising R-curves. This concept may also be applicable to crack tip shielded materials, such as zirconias, if a shielding degradation process can be identified for them or if frontal zone shielding can somehow be coupled to bridging in the crack wake. In principle, the approach utilized in this paper makes it feasible to predict crack growth rates in fatigue from knowledge of basic micromechanics. One simply needs a good model describing how the shielding zone characteristics (i.e., σ or τ distribution and zone size) change as the crack grows under given cyclic loading conditions. However, to arrive at such a model one must first solve complex problems relating each increment of cyclic loading to displacement, wear, and bridge failure within the shielding zone.

The above picture has emphasized mechanical equilibrium and has ignored nonequilibrium conditions, where $dK_{sh} \neq 0$, as well as kinetic factors influencing fatigue crack propagation. Environmental interactions (i.e., static fatigue) must be considered to evaluate situations involving this thermally activated kinetic process. In addition to promoting subcritical crack growth, environment may modify the initial features of the R-curve by altering the details of bond scission and debonding. Environment may also affect shielding degradation via frictional wear, providing another possible rationalization for environmental effects on cyclic fatigue. In addition, characterization of dK_{sh}, $\partial K_{sh}/\partial a$, and $\partial K_{sh}/\partial t$ under nonequilibrium conditions, where these quantities change over time, is also possible. By incorporating these factors into the framework set out in this paper, accurate predictions should result for cyclic fatigue under more general conditions.

VI. Conclusions

(1) Steady-state shielding is established during cyclic fatigue under constant K_{max} and R-ratio test conditions. This develops within a crack growth increment of about 200 μm for the gas-pressure-sintered Si_3N_4 material tested here.

(2) Steady-state cyclic fatigue may be regarded as a mechanical equilibrium for which the net change in shielding, dK_{sh}, is zero. This equilibrium appears to reflect a balance between a shielding accumulation process resulting from crack growth and a shielding degradation process resulting from frictional wear of sliding interfaces behind the crack tip.

(3) A "cyclic" R-curve has been found which describes the $\partial K_{sh}/\partial a$ response of our material after cyclic loading, and which is distinguishable from a monotonic R-curve. The difference probably arises from different distributions of crack face tractions and displacements in the shielding zone produced by cyclic and monotonic loading.

(4) The rate of shielding accumulation for a growing crack under cyclic fatigue, $\partial K_{sh}/\partial a$, is a strong function of the K_{max} used to obtain steady state. This strong K_{max} dependence is related to the "cyclic" R-curve, and it can account for the strong K_{max} dependence of da/dt observed experimentally for cyclic fatigue in ceramics.

(5) The rate of shielding degradation, $\partial K_{sh}/\partial t$, during cyclic fatigue is only weakly dependent on the stress intensity range, ΔK. This is rationalized by the weak ΔK dependence of the cyclic crack opening displacement, which governs wear and shielding degradation rates during cyclic loading. This degradation process can account for the weak ΔK dependence of da/dt observed experimentally.

APPENDIX

Derivation of $\partial \tau/\partial u$ from a Wear Law

The following is a first-order approximation for $\partial \tau/\partial u$ based on wear considerations. We first assume the shear stress between two sliding grains is described by the Coulomb law

$$\tau = \mu \sigma_{rr} \tag{A–1}$$

where σ_{rr} is the radial compressive stress acting on the grain (Poisson's ratio effects are assumed to be negligible). Tests on ceramic/ceramic tribological couples indicate that μ is often constant over a considerable period of time and sliding distance.[43,44] Warren *et al.*[19] have also inferred this from single-fiber pushout tests. Then, by identifying σ_{rr} with a misfit strain, ε_{ms}, due to thermal expansion anisotropy, surface roughness, etc., we can expect wear to reduce σ_{rr} and hence τ. This can be shown by letting

$$\sigma_{rr} = C'E\,\varepsilon_{ms} \tag{A–2}$$

and thus

$$\frac{\partial \tau}{\partial u} = \mu \frac{\partial \sigma_{rr}}{\partial u} = \mu C'E \frac{\partial \varepsilon_{ms}}{\partial u} \tag{A–3}$$

where E is Young's modulus and C' is a correction factor (which equals $1/(2 - 2\nu)$ for the case of a fiber in an infinite matrix,[45] where ν is Poisson's ratio). Since the misfit strain changes as material wears away at the interface, we can write

$$d\varepsilon_{ms} = \frac{-dW_L}{R} \tag{A–4}$$

where R is the radius of the grain and $-dW_L$ represents the incremental linear wear. We assume an incremental linear wear law of the form

$$\frac{dW_L}{du} = kP = k\sigma_{rr}\pi R^2 \tag{A–5}$$

where P is the normal load, identifiable with σ_{rr}, and k is a wear constant with units m/N. Combining Eqs. (A–1) to (A–4), we arrive at

$$\frac{\partial \tau}{\partial u} = \left(\frac{\mu C'E}{R}\right)\left(\frac{-dW_L}{du}\right)$$
$$= -kC'E\pi R\tau = -k'\tau \tag{A–6}$$

where k' includes all the constant terms. This implies an exponential decay of τ, which would be consistent with data reported by Holmes and Cho[23] for ceramic matrix composites.

Acknowledgments: We would like to thank Drs. T. Y. Tien and K. R. Lai for providing the material used in this study.

References

[1]S. Y. Liu and I-W. Chen, "Fatigue of Yttria-Stabilized Zirconia II: Crack Propagation, Fatigue Striations, and Short Crack Behavior," *J. Am. Ceram. Soc.*, **74** [6] 1206–18 (1991).

[2]R. H. Dauskardt, M. R. James, J. R. Porter, and R. O. Ritchie, "Cyclic Fatigue-Crack Growth in a Silicon Carbide Whisker-Reinforced Alumina Ceramic Composite: Long- and Small-Crack Behavior," *J. Am. Ceram. Soc.*, **75** [4] 759–71 (1992).

[3]R. H. Dauskardt, B. J. Dalgleish, D. Yao, and R. O. Ritchie, "Cyclic Fatigue-Crack Growth in a Silicon Carbide Whisker-Reinforced Alumina Ceramic Composite: Role of Load Ratio," *J. Mater. Sci.*, **28** [12] 3258–66 (1993).

[4]R. H. VanStone, "Residual Life Prediction Methods for Gas Turbine Components," *Mater. Sci. Eng.*, **A103**, 49–61 (1988).

[5]P. L. Swanson, C. J. Fairbanks, B. R. Lawn, Y.-W. Mai, and B. J. Hockey, "Crack-Interface Grain Bridging as a Fracture Resistance Mechanism in Ceramics: I, Experimental Study on Alumina," *J. Am. Ceram. Soc.*, **70** [4] 279–89 (1987).

[6]Y.-W. Mai and B. R. Lawn, "Crack-Interface Grain Bridging as a Fracture Resistance Mechanism in Ceramics: I, Theoretical Fracture Mechanics Model," *J. Am. Ceram. Soc.*, **70** [4] 289–94 (1987).

[7]G. Vekinis, M. F. Ashby, and W. R. Beaumont, "*R*-Curve Behavior of Al_2O_3 Ceramics," *Acta Metall. Mater.*, **38** [6] 1151–62 (1990).

[8]J. Rodel, J. F. Kelly, and B. R. Lawn, "In Situ Measurements of Bridged Crack Interfaces in the Scanning Electron Microscope," *J. Am. Ceram. Soc.*, **73** [11] 3313–18 (1990).

[9]A. Reichl and R. W. Steinbrech, "Determination of Crack-Bridging Forces in Alumina," *J. Am. Ceram. Soc.*, **71** [6] C-299–C-301 (1988).

[10]Y. Maniette, M. Inagaki, and M. Sakai, "Fracture Toughness and Crack Bridging of a Silicon Nitride Ceramic," *J. Eur. Ceram. Soc.*, **7**, 255–63 (1991).

[11]S. J. Bennison and B. R. Lawn, "Role of Interfacial Grain-Bridging Sliding Friction in Crack-Resistance and Strength Properties of Non-Transforming Ceramics," *Acta Metall. Mater.*, **37** [10] 2659–71 (1989).

[12]P. F. Becher, H. T. Lin, S. L. Hwang, M. J. Hoffmann, and I-W. Chen, "The Influence of Microstructure on the Mechanical Behavior of Silicon Nitride Ceramics"; pp. 147–58 in *Silicon Nitride Ceramics, Scientific and Technological Advances*, Materials Research Society Symposium Proceedings, Vol. 287. Edited by I-W. Chen, P. F. Becher, M. Mitomo, G. Petzow, and T.-S. Yen. Materials Research Society, Pittsburgh, PA, 1993.

[13]P. F. Becher, "Crack Bridging Processes in Toughened Ceramics"; pp. 19–33 in *Toughening Mechanisms in Quasi-Brittle Materials*. Edited by S. P. Shah. Kluwer Academic Publishers, Dordrecht, Netherlands, 1991.

[14]R. W. Steinbrech, A. Reichl, and W. Schaarwachter, "*R*-Curve Behavior of Long Cracks in Alumina," *J. Am. Ceram. Soc.*, **73** [7] 2009–15 (1990).

[15]A. G. Evans and D. B. Marshall, "The Mechanical Behavior of Ceramic Matrix Composites," *Acta Metall.*, **37** [10] 2567–83 (1989).

[16]R. A. Kerans and T. A. Parthasarathy, "Theoretical Analysis of the Fiber Pullout and Pushout Tests," *J. Am. Ceram. Soc.*, **74** [7] 1585–96 (1991).

[17]T. P. Weihs and W. D. Nix, "Experimental Examination of the Push-Down Technique for Measuring the Sliding Resistance of Silicon Carbide Fibers in a Ceramic Matrix," *J. Am. Ceram. Soc.*, **74** [3] 524–34 (1991).

[18]A. Dollar and P. S. Steif, "Cohesive Zone Approach to Interpreting the Fiber Push-Out Test," *J. Am. Ceram. Soc.*, **76** [4] 897–903 (1993).

[19]P. D. Warren, T. J. Mackin, and A. G. Evans, "Design, Analysis, and Application of an Improved Push-through Test for the Measurement of Interface Properties in Composites," *Acta Metall. Mater.*, **40** [6] 1243–49 (1992).

[20]H. Cai, K. T. Faber, E. R. Fuller, Jr., "Crack Bridging by Inclined Fibers/Whiskers in Ceramic Composites," *J. Am. Ceram. Soc.*, **75** [11] 3111–17 (1992).

[21]S. Lathabai, J. Rodel, and B. R. Lawn, "Cyclic Fatigue from Frictional Degradation at Bridging Grains in Alumina," *J. Am. Ceram. Soc.*, **74** [6] 1340 (1991).

[22]A. W. Pryce and P. A. Smith, "Matrix Cracking in Unidirectional Ceramic Matrix Composites under Quasi-Static and Cyclic Loading," *Acta Metall. Mater.*, **41** [4] 1269–81 (1993).

[23]J. W. Holmes and C. Cho, "Experimental Observations of Frictional Heating in Fiber-Reinforced Ceramics," *J. Am. Ceram. Soc.*, **75** [4] 929–38 (1992).

[24]D. B. Marshall and W. C. Oliver, "Measurement of Interfacial Mechanical Properties in Fiber-Reinforced Ceramic Composites," *J. Am. Ceram. Soc.*, **70** [8] 542–48 (1987).

[25]X. Hu and Y.-W. Mai, "Crack-Bridging Analysis for Alumina Ceramics under Monotonic and Cyclic Loading," *J. Am. Ceram. Soc.*, **75** [4] 848–53 (1992).

[26]R. H. Dauskardt, D. B. Marshall, and R. O. Ritchie, "Cyclic Fatigue-Crack Propagation in MgO-PSZ Ceramics," *J. Am. Ceram. Soc.*, **73** [4] 893–903 (1990).

[27]D. S. Jacobs and I-W. Chen, "Mechanical and Environmental Factors in the Cyclic and Static Fatigue of Silicon Nitride," *J. Am. Ceram. Soc.*, **77** [5] 1153–61 (1994).

[28]S. Horibe, "Cyclic Fatigue Damage and Microstructure of Ceramic Materials," *Proc. Int. Conf. Fatigue Fatigue Thresh., 4th*, **2**, 753–58 (1990).

[29]J. Homeny and W. L. Vaughn, "*R*-Curve Behavior in a Silicon Carbide Whisker/Alumina Matrix Composite," *J. Am. Ceram. Soc.*, **73** [7] 2060–62 (1990).

[30]A. Ueno, H. Kishimoto, H. Kawamoto, and M. Asakura, "Crack Propagation Behavior of Sintered Silicon Nitride under Cyclic Load of High Stress Ratio and High Frequency"; see Ref. 28, pp. 733–38.

[31]H. Kishimoto, A. Ueno, and H. Kawamoto, "Crack Propagation Behavior of Si_3N_4 under Cyclic Loads—Influence of Difference in Materials"; see Ref. 28, pp. 727–32.

[32]C.-W. Li, D.-J. Lee, and S.-C. Lui, "*R*-Curve Behavior and Strength for In-Situ Reinforced Silicon Nitrides with Different Microstructures," *J. Am. Ceram. Soc.*, **75** [7] 1777–85 (1992).

[33]P. Chantikul, S. J. Bennison, and B. R. Lawn, "Role of Grain Size in the Strength and *R*-Curve Properties of Alumina," *J. Am. Ceram. Soc.*, **73** [8] 2419–27 (1990).

[34]N. P. Padture and H. M. Chan, "Improved Flaw Tolerance in Alumina Containing 1 vol% Anorthite via Crystallization of the Intergranular Glass," *J. Am. Ceram. Soc.*, **75** [7] 1870–75 (1992).

[35]D. B. Marshall and M. V. Swain, "Crack Resistance Curves in Magnesia-Partially-Stabilized Zirconia," *J. Am. Ceram. Soc.*, **71** [6] 399–407 (1988).

[36]C.-W. Li and J. Yamanis, "Super-Tough Silicon Nitride with *R*-Curve Behavior," *Ceram. Eng. Sci. Proc.*, **10** [7–8] 632–45 (1989).

[37]C.-H. Hsueh and P. F. Becher, "Evaluation of Bridging Stress from *R*-Curve Behavior for Nontransforming Ceramics," *J. Am. Ceram. Soc.*, **71** [5] C-234–C-237 (1988).

[38]A. Okada and N. Hirosaki, "Subcritical Crack Growth in Sintered Silicon Nitride Exhibiting a Rising *R*-Curve," *J. Am. Ceram. Soc.*, **73** [7] 2095–96 (1990).

[39]J. A. Salem and J. L. Shannon Jr., "Fracture Toughness of Si_3N_4 Measured with Short Bar Chevron-Notched Specimens," *J. Mater. Sci.*, **22** [1] 321–24 (1987).

[40]P. F. Becher, "Microstructural Design of Toughened Ceramics," *J. Am. Ceram. Soc.*, **74** [2] 255–69 (1991).

[41]S. Y. Liu and I-W. Chen, "Fatigue Deformation Mechanisms in Zirconia Ceramics," *J. Am. Ceram. Soc.*, **75** [5] 1191–206 (1992).

[42]D. B. Marshall, B. N. Cox, and A. G. Evans, "The Mechanics of Matrix Cracking in Brittle-Matrix Fiber Composites," *Acta Metall. Mater.*, **33** [11] 2013–21 (1985).

[43]D. Klaffke and K. H. Habig, "Fretting Wear Tests of Silicon Carbide," *Wear Mater.*, Vol. 1, 361–70 (1987).

[44]O. O. Ajayi and K. C. Ludema, "Formation of Transfer Film during Ceramics/Ceramics Repeat Pass Sliding," *Wear Mater.*, Vol. 1, 349–59 (1989).

[45]B. Budiansky, J. W. Hutchinson, and A. G. Evans, "Matrix Fracture in Fiber-Reinforced Ceramics," *J. Mech. Phys. Solids*, **34** [2] 167–89 (1986). □